NANO LETTERS

Letter

pubs.acs.org/NanoLett

Alternative Route to Silicene Synthesis via Surface Reconstruction on h-$MoSi_2$ Crystallites

Cameron Volders, Ehsan Monazami, Gopalakrishnan Ramalingam, and Petra Reinke*

Department of Materials Science and Engineering, University of Virginia, 395 McCormick Road, Charlottesville, Virginia 22904, United States

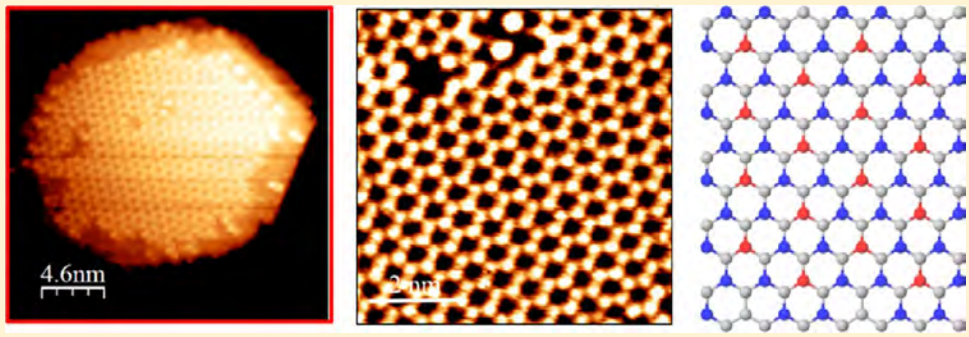

ABSTRACT: Silicene is a two-dimensional material with a Dirac-type band structure and it is particularly attractive due to its potential for integration with Si-based technology. The primary focus has been to grow single silicene layers and understand how the electronic structure is affected by the substrate and the phase transition between low- and high-buckling configurations. Typically, silicene is synthesized by depositing monolayer amounts of silicon onto a heated Ag(111) surface; however, other growth substrates such as Ir(111) and ZrB_2 have been studied recently. We present a novel route for silicene synthesis via a high-temperature surface reconstruction of hexagonal-$MoSi_2$ nanocrystallites. The h-$MoSi_2$ crystallites are formed by annealing of thin Mo-layers on Si(100)-(2 × 1) and their crystallographic orientation is controlled via an epitaxial relation with the Si-substrate. The (0001) plane of h-$MoSi_2$ is comprised of Si-hexagons with a Mo atom residing in the center. Annealing above approximately 650 °C causes the (0001) plane to undergo a surface reconstruction process leaving a honeycomb pattern on the surface of these crystallites as shown by scanning tunneling microscopy. We define this surface layer as a silicene-like reconstruction (SLR), and a detailed geometric analysis of our structure yields a perfect match with the $(\sqrt{3} \times \sqrt{3})R30°$ silicene superstructure in a low-buckled configuration ($AB\bar{A}$). Scanning tunneling spectroscopy data of the SLR, Si(001)-(2 × 1) and h-$MoSi_2$ surfaces agree with this interpretation. The formation of this structure on a transition metal silicide opens up the opportunity for integration into Si-based devices without the necessity for a transfer scheme.

KEYWORDS: *Silicene, scanning tunneling microscopy, disilicide, reconstruction, Si(001)*

A wide range of 2D materials have been discovered and synthesized in the past decade starting with graphene, which remains one of the most intensely studied material despite its challenges with respect to integration in conventional transistor architecture. In recent years, other 2D materials such as the family of transition metal dichalcogenides (TMDs), silicene, germanene and stanene have come into focus.[1−5] Silicene is particularly interesting because it has been shown to possess a honeycomb structure and, consequently, a Dirac-type behavior is expected.[6−10] The spin−orbit coupling opens a very small band gap, which might be increased by application of a vertical electric field.[3] The Dirac-type behavior requires a low-buckled silicene layer, while the band structure for the highly buckled configuration approaches parabolic bands characteristic of Si(111).[11,12] Perfectly flat silicene with a pure sp^2 type bonding is energetically unfavorable and has not been observed. The substrate and its electronic structure play a critical role in the stabilization of the desired low-buckled silicene structure. Ag(111) is still the most frequently used substrate material because it is an epitaxial template with hexagonal surface symmetry and does not form a silicide.[6,8,13−15] More recently the segregation of Si, which is used as a substrate, to the surface of ZrB_2 thin films, and the deposition of Si on MoS_2 have been reported as methods for silicene and silicene nanoribbon synthesis, respectively.[16−18]

We show in the present study that the hexagonal phase of $MoSi_2$ has a high temperature (>650 °C) surface reconstruction with the characteristics of low-buckled silicene. Our interest in $MoSi_2$ was motivated by interest in the initial stages of silicide oxidation. $MoSi_2$ nanocrystals were synthesized on Si(001)-(2 × 1) by a solid state epitaxy process, which lead to the discovery of a silicene-like reconstruction (SLR) on the h-$MoSi_2$(0001) surface. The geometric and electronic structure of the SLR were studied with scanning tunneling microscopy

Received: September 28, 2016
Revised: December 18, 2016
Published: December 20, 2016

DOI: 10.1021/acs.nanolett.6b04065
Nano Lett. 2017, 17, 299−307

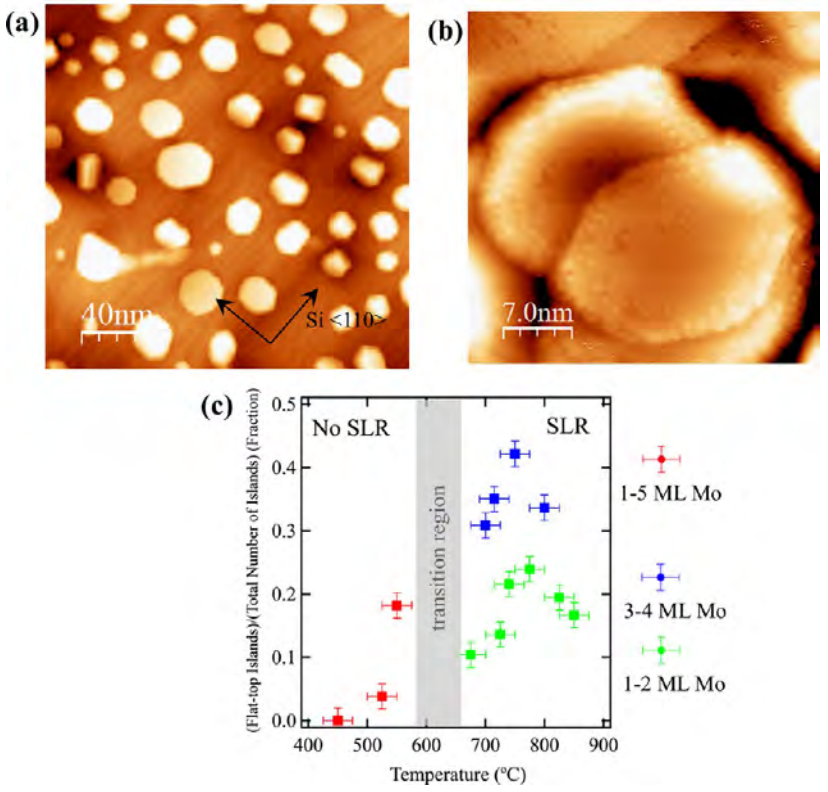

Figure 1. (a) Representative section of the Si(001)-(2 × 1) surface with a mixture of $MoSi_2$ crystallites for a sample annealed at 750 °C. (b) Flat-top crystallites, which corresponds to the h-$MoSi_2$(0001) surface showing the honeycomb structure of the silicene-like reconstruction (SLR). The image was taken with a double tip and the crystallite has therefore a "ghost", which can be recognized by the identical defect and rim structures. The double tip does not impact imaging of the flat Si(001) surface. (c) Parameter space graph summarizing all deposition experiments, which depicts the percentage of flat-top islands as a function of temperature and amount of Mo deposited prior to annealing.

(STM) and spectroscopy (STS). Our analysis of the SLR supports the analogy between the SLR and silicene, which is decoupled from the $MoSi_2$. This work opens a new pathway to silicene synthesis and its integration in semiconductor device structures.

The experiments were performed in a ultrahigh vacuum (UHV) preparation chamber that is connected to a scanning tunneling microscope (Omicron Nanotechnology VT-SPM) with a base pressure of $<2 \times 10^{-10}$ mbar. P-type single crystal Si(001) samples with a resistivity of 0.01−0.02 (Ω·cm) were annealed via direct current heating overnight at ∼450 °C followed by repeated flashing to ∼1200−1300 °C until a high quality (2 × 1) reconstruction was observed with STM. Molybdenum was deposited by electron-beam evaporation from a Mantis mini e-beam evaporator using a 99.9% purity Mo rod from American Elements. The deposition rate was between 0.4−1 ML/min and calibrated using a quartz crystal monitor. For each experiment, 1−5 monolayers (ML), 0.6 to 1.5 nm, of Mo were deposited on the Si (001)-(2 × 1) substrate surface at room temperature. The Mo-layers as deposited show a granular structure with small Mo clusters,[19] which completely cover the Si surface. The Si samples are then heated to 400−900 °C for 5−15 min. The temperature was measured with a pyrometer and the error is about ±15 °C due to the small size of the sample. The samples were then cooled to room temperature followed by STM and STS (scanning tunneling spectroscopy) studies.

All measurements were performed at room temperature in constant current mode with electrochemically etched tungsten tips. The typical imaging conditions for Si (001) were V = (−1.5 to −2.25 V) with a tunneling current of I = 0.03−0.1 nA. The same range of imaging conditions were used for the $MoSi_2$ nanostructures and the SLR and the images are nearly insensitive to choice of imaging conditions. The STS measurements were performed within spectroscopy maps. For spectroscopy maps, at every fifth pixel I/V characteristics are measured with an open feedback loop in the voltage interval −2 to 2 V. The feedback loop is engaged for the intermediate pixels where the topography is recorded as usual. The I/V curves are numerically differentiated and normalized $dI/dV/(I/V + \varepsilon)$ following the procedure described by Feenstra et al.[20] STM images were analyzed using Gwyddion[21] and WSxM,[22] which are open source software packages for SPM data analysis.

The Mo−Si phase diagram includes three stable line compounds Mo_5Si_3, Mo_3Si, and $MoSi_2$, and the presence of the large Si reservoir promotes the formation of the disilicide $MoSi_2$.[23−26] Two phases of $MoSi_2$ have been identified, tetragonal $C11_b$ and hexagonal C40. The tetragonal phase is the thermodynamically stable phase, whereas the hexagonal phase is a metastable phase readily observed when silicide crystallites are grown as nanometer-scale islands or thin films. A representative example illustrating size and shape distribution of silicide crystallites obtained after annealing at 750 °C is shown in Figure 1a. Some of crystallites are slightly burrowed into the Si surface indicating a significant surface mobility of Mo that drives the solid-state reaction with Si and leaves large sections of the Si-surface in its pristine (2 × 1) reconstruction.[27] The crystallite sizes vary from 10 to 100 nm in diameter depending on the Mo coverage and annealing temperature. The $MoSi_2$ crystallites are in contact with the Si(001) surface and have a

DOI: 10.1021/acs.nanolett.6b04065
Nano Lett. 2017, 17, 299−307

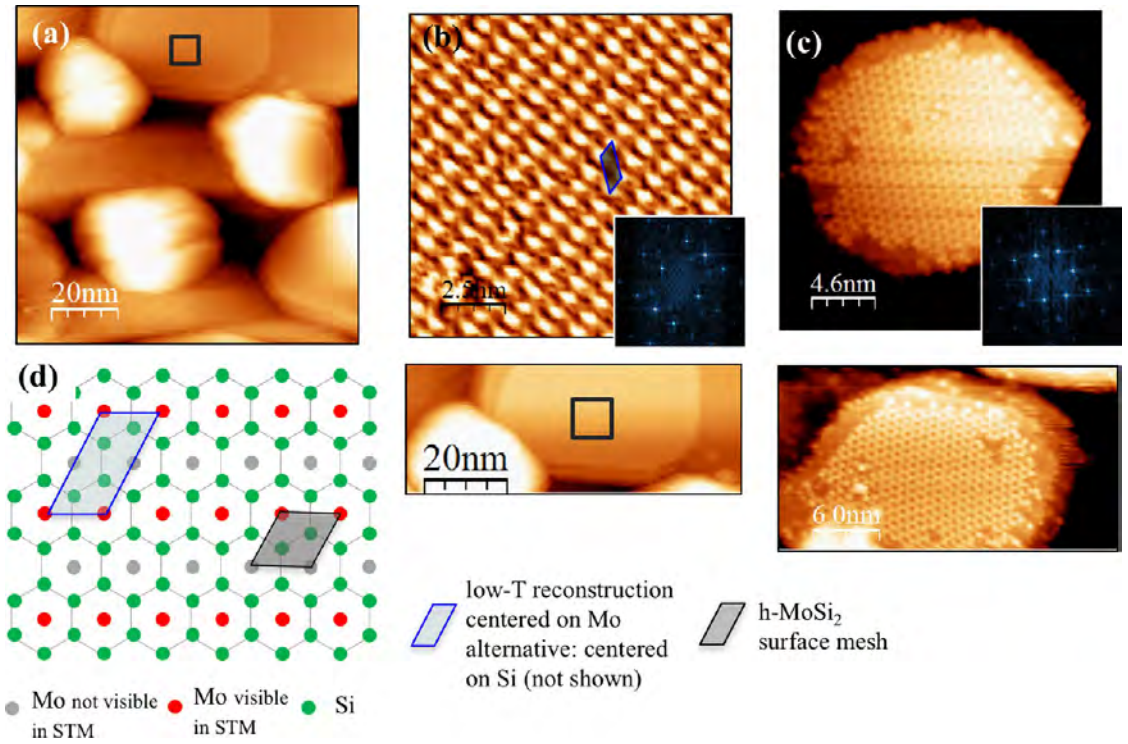

Figure 2. (a) Image of $MoSi_2$ crystallites with an h-$MoSi_2$(0001) crystallite showing the low-T reconstruction. (b) Atomically resolved images of low-T reconstruction and enlarged section of surface from (a). The image of the reconstruction was obtained in the area marked by a square. (c) SLR reconstruction on two different crystallites. The corresponding fast Fourier transforms illustrate the change in surface mesh symmetry. (d) Schematic of the h-$MoSi_2$(0001) surface with the hexagonal Si arrangement and Mo-atoms at the center of each hexagon. The surface unit cell of the unreconstructed surface is indicated. One of the possible unit cells of the low-T reconstruction centered on the Mo surface atoms is indicated: Mo-atoms visible in STM images are marked in red, those which would not be visible in the STM image are marked in gray. An alternative surface unit cell can be centered on the Si surface atoms yielding identical interatomic distances but would require that the Mo atoms are not visible in the STM images.

height of several nanometers (on average between 2 and 6 nm with respect to the Si-surface). The surface reconstructions discussed in the next paragraph are therefore not in contact with the Si(001) surface. However, the $MoSi_2$ crystallites have a well-defined epitaxial relation to the Si(001) surface expressed in their hexagonal habit. The orientation of the low-T and SLR are on the other hand linked to the $MoSi_2$ surface structure and thus always show the same orientation with respect to the underlying Si(001) surface. H-$MoSi_2$ crystallites can be recognized by their hexagonal crystal habit and "flat top" surface as visualized in the Figures 1a,b. The "flat top" surface of the h- $MoSi_2$ corresponds to the (0001) plane, which is parallel to the Si (001) surface in agreement with the preferred epitaxial relations.[24−26,28]

Figure 1c summarizes the parameter space for the synthesis of "flat top islands", or h-$MoSi_2$ crystallites. The graph relates the percentage of "flat top" hexagonal islands to deposition conditions defined by temperature and initial Mo-coverage. Each marker represents a separate experiment underscoring the reproducibility of h-$MoSi_2$ synthesis. The total number of islands in a sample includes both hexagonal and tetragonal islands from several images and the analysis includes between 90 and 300 islands for T > 650 °C, 616 islands for the 520 °C data point, and the data point at 550 °C has by far the lowest count with only 11 crystallites. Figure 1a is a representative image for the sample with the largest contribution of h-$MoSi_2$ (0001) of nearly 50% (750 °C for an initial Mo coverage of 3−4 ML Mo). All of these crystallites show the SLR reconstruction. At higher initial Mo coverage >5 ML the islands start to coalesce, which leads to the formation of a continuous film with a mixture of phases and orientations not suitable for a statistical analysis.

All h-$MoSi_2$ (0001) surfaces for annealing temperatures of 670 °C and above possess the honeycomb surface structure, henceforth labeled as the silicene-like reconstruction (SLR) seen in Figure 1b. The presence of the SLR is independent of island size and is solely controlled by annealing temperature. The h-$MoSi_2$ (0001) surface shows a different reconstruction at lower temperatures, which is included in Figure 2. The preferential orientation of the h-$MoSi_2$ islands with respect to the Si surface (Figure 1a) leads to a preferential orientation of the SLR. Figure 2 provides atomically resolved images of hexagonal islands containing the low-T reconstruction and the SLR along with their corresponding FFT patterns. The honeycomb symmetry of the SLR is clearly visible in both the topography image and FFT pattern, whereas the island without the SLR (low-T reconstruction) displays an oblique rectangular symmetry. The filled state images for the low-T reconstruction and the SLR were taken with identical imaging conditions (V_{bias} = −2.0 V and I_t = 0.1 nA). Figure 2a,c illustrates another significant difference: the SLR always possesses a readily apparent "rim" and exposes a structurally and electronically distinct region close to the edge of the crystallite. The low-T reconstruction always terminates right at the edge of the crystallite. The low-T reconstruction fits very well with the geometry of the $MoSi_2$ (0001) surface as shown in Figure 2d, where each Si-hexagon is centered around a Mo atom. Superimposing the STM image on the surface structure

DOI: 10.1021/acs.nanolett.6b04065
Nano Lett. 2017, 17, 299−307

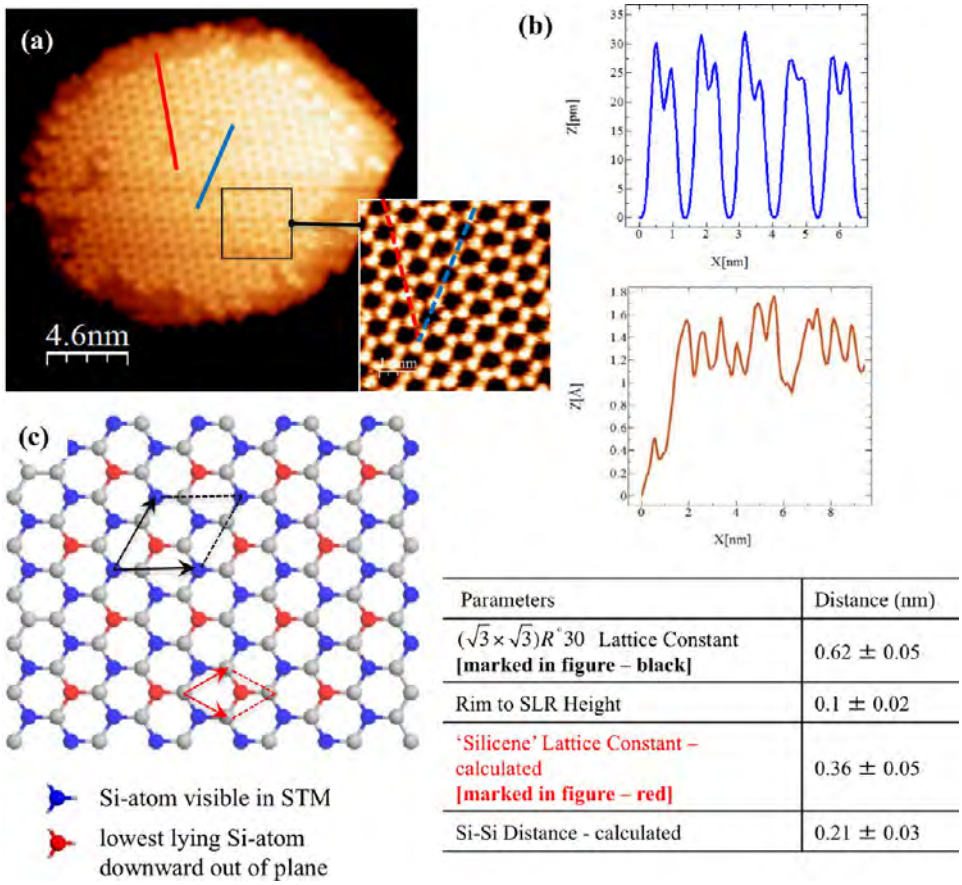

Parameters	Distance (nm)
$(\sqrt{3}\times\sqrt{3})R^{\circ}30$ Lattice Constant **[marked in figure – black]**	0.62 ± 0.05
Rim to SLR Height	0.1 ± 0.02
'Silicene' Lattice Constant – calculated **[marked in figure – red]**	0.36 ± 0.05
Si-Si Distance - calculated	0.21 ± 0.03

Figure 3. Analysis of the SLR geometry: (a) STM image of a representative crystallite, which shows the SLR; (b) linescans along high symmetry lines on the surface as marked in the image. The equivalent directions of the linescan are illustrated in a high-resolution image. (c) Model of the SLR reconstruction: the unit cell of the SLR, which corresponds to the $(\sqrt{3}\times\sqrt{3})R^{\circ}30$ silicene structure (black), and the silicene lattice constant, which corresponds to lattice constant of the honeycomb mesh (red), are indicated. The buckling given in the table (d) refers to the measured apparent height between the perimeter of the hexagons in the SLR and the center of the hexagons (red linescan).

yields a perfect fit if each protrusion in the image is positioned on every second Mo-atom. However, the agreement is equally good if we move the unit cell to match Si-surface atoms, although this would require all Mo atoms to be invisible in STM. A unique assignment cannot be confirmed at present. The excellent match in this purely geometric assessment indicates the surface of h-$MoSi_2$ crystallites is terminated by the (0001) plane of the C40 crystal structure. The reconstruction is likely dominated by slight vertical displacements leading to the selective imaging of some surface atoms (every second Mo atom or every fourth Si atom). An alternative interpretation for the atom selective image contrast is that only atoms with specific bonding configurations to the subsurface layers are imaged due to subtle variations in the local density of states. Some rare earth disilicides such as $ErSi_2/ErSi_{1.7}$ exhibit surface reconstruction with hexagonal symmetry, where every second Si atom is visible in the STM.[29−35] The electronic structure of the rare earth disilicide surfaces does not exhibit a Dirac cone type signature, which is likely due to strong coupling with the underlying substrate. No phase mixtures between the low-T surface and the SLR are observed.

Figure 3 provides a more detailed description of the SLR structure. The inset in Figure 3a is an atomically resolved STM image revealing the honeycomb pattern and Figure 3c provides a model, which illustrates the surface structure of the SLR. Linescans were performed to determine the lattice constant of the SLR along with other geometric parameters, which is provided in the table of Figure 3. These values were averaged over >60 linescans using different crystallites yielding the dimensions of the lattice constant of the SLR to be 0.62 ± 0.05 nm defined by the atoms visible in the STM images. We propose the SLR is made by a surface reconstruction of the h-$MoSi_2$ (0001) plane where the Si atoms become decoupled from the underlying surface and adopt the honeycomb structure reducing the Si−Si bond length at the same time. The (0001) plane adopts this structure as it is most energetically favorable because it minimizes the surface energy by complete saturation of the Si-atom bonding. It is facilitated by the (0001) structure where the Si atoms are already arranged in hexagons. The honeycomb pattern is created with two Si atoms out of every Si-hexagon being buckled upward out of plane, and one Si atom is buckled downward into the plane, which has been named an $AB\bar{A}$ configuration by Feng et al. and is realized in the $(\sqrt{3}\times\sqrt{3})R30^{\circ}$ reconstruction on Ag(111). A model of this superstructure is shown in Figure 3c. As a consequence of buckling, not all Si atoms are visible in STM but only every third Si atom (2 out of 6) can be visualized. The dimensions of the reconstruction are summarized in the table and the lattice constant of the potential underlying silicene structure and Si−Si distances are calculated from the STM measurements. These values are all in excellent agreement with $(\sqrt{3}\times\sqrt{3})R30^{\circ}$ silicene as it is grown on Ag(111)[13] and

DOI: 10.1021/acs.nanolett.6b04065
Nano Lett. 2017, 17, 299−307

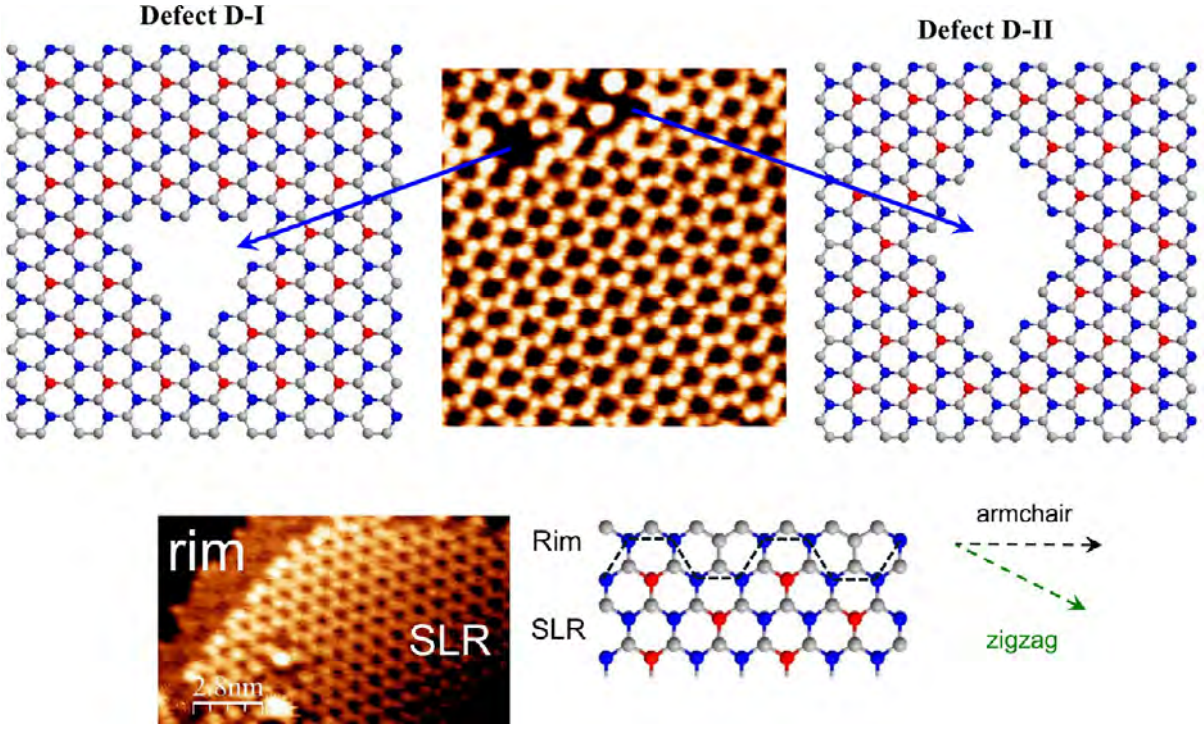

Figure 4. (a) Defect motifs observed on the SLR with a direct comparison between the STM image and the structure models. (b) High-resolution image of a section of the SLR rim with the corresponding structure model.

match with theoretical predictions for silicene.[11] We use the designation $(\sqrt{3} \times \sqrt{3})R30°$−SLR in analogy to the structure reported in the literature for silicene layers on Ag(111), while retaining the descriptor SLR until the Dirac nature of a decoupled silicene layer on the h-$MoSi_2$ crystallites can be confirmed unequivocally. Alternative scenarios in the interpretation of the SLR are as follows: (i) A coincidence lattice leading to a moiré pattern, which is formed by a lattice mismatch between substrate and 2D material; this would yield the atomic scale and the moire periodic lattice in the same image, which is not seen in the high-resolution STM images. (ii) A regular lattice of defects that are positioned between the top layer and the $MoSi_2$ crystal lattice; this model is akin to the $ErSi_{1.7}$ surfaces. However, this model cannot explain the appearance of a rim in all SLR reconstructions. In summary, the low-T reconstruction is a reconstruction of the (0001) plane of h-$MoSi_2$ but the lower temperature does not allow Si to separate from the surface and thus the SLR is favored at higher temperatures.

The SLR lattice constant is larger than the h-$MoSi_2$ lattice constant (0.464 nm),[26,28] and the calculated Si−Si distance in the $(\sqrt{3} \times \sqrt{3})R30°$ configuration is smaller than the Si−Si distance in the h-$MoSi_2$ (0001) plane. No modulation of the apparent height by moiré-type patterns is observed, which is in agreement with an overall weak bonding of the SLR to the h-$MoSi_2$. The analysis of characteristic defect motifs (D) and the rim of the SLR are additional evidence for the assignment of the SLR structure as discussed above. These defects always occur on the SLR layers and are never observed in the low-T reconstruction. Figure 4 includes several representative defect motifs, D-I and D-II, and their corresponding structure based on the SLR, which determines the shape of their boundaries. Note that D-I is exactly one-half of D-II. Overall the distinct shape of the defects in relation to the SLR supports our interpretation that the hexagon superlattice visible in the STM images corresponds geometrically to the $(\sqrt{3} \times \sqrt{3})R30°$ silicene reconstruction. Occasionally the defect motif includes exceptionally "bright" atoms as seen in D-II, which might be dangling bonds. Some segments of the SLR perimeter show a termination of the $(\sqrt{3} \times \sqrt{3})R30°$ with an armchair geometry as illustrated in Figure 4.

All crystallites with an SLR are surrounded by a rim area, which marks the boundary of the crystallite. In contrast, this rim area is never seen in the low-T reconstruction and holds significance for the interpretation of the surface structure and buckling. The height of the SLR at the rim is ∼0.1 nm while the depth of the defects is only ∼0.045 nm. The defects in the SLR can be described as a local breakdown of the reconstruction where Si atoms are missing. We have not been able to achieve atomic resolution inside the defects, or on the rim area. Another critical aspect in assessing the SLR (and silicene) is the determination of the extent of buckling in the honeycomb structure. Silicene, unlike graphene, is not flat but presents in different phases, which are distinguished by their degree of buckling.[12,36] The highly coveted Dirac-type band structure features are only realized in configurations with a low-buckling configuration controlled by sp^2 type hybridization.[11,12]

One approach to the measurement of the degree of buckling in silicene layers has been the use of STM linescans, and the height differential is directly associated with the amount of buckling. This provides some insight but can only be a rough estimate considering STM height measurements are always modulated by the local density of states. Our STM measurements (Figure 3) yield values close to those given in the literature for a low buckling configuration. The presence of a rim, which is seen at the perimeter of all SLR structures, but not in low-T reconstruction, holds additional information on the degree of SLR buckling. An additional method to assess the degree of buckling in the SLR structure is based on the area associated with the SLR and total surface area of the crystallite

DOI: 10.1021/acs.nanolett.6b04065
Nano Lett. 2017, 17, 299−307

(Rim + SLR). We have proposed a surface reconstruction process that decouples the Si atoms from the underlying h-$MoSi_2$ crystallites and argue they must buckle inward to create the observed rim structure around the SLR. Therefore, the area of each SLR structure on crystallites of different size can be used to quantify the degree of buckling assuming all Si atoms from the h-$MoSi_2$ (0001) plane are conserved in this process. For example, a larger rim area and the more an SLR "shrinks" inward would equate a higher degree of buckling.

Figure 5 provides an area comparison between the measured area of the SLR structures on different sized crystallites to a

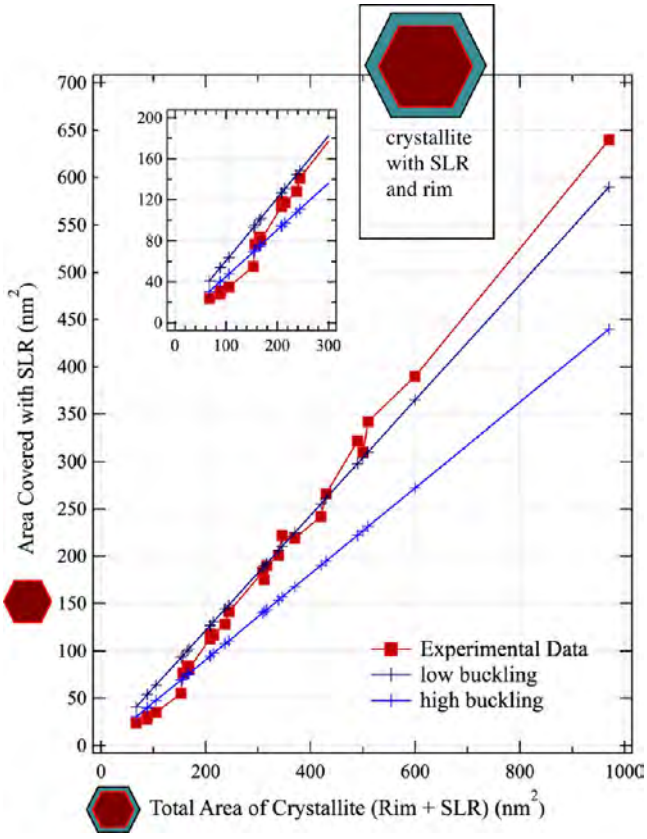

Figure 5. SLR area on the h-$MoSi_2$(0001) "flat top" crystallites as a function of the total area, which is the sum of SLR and rim area. The surface coverage for a high-buckling silicene (blue) and a low buckling silicene phase (purple) are shown; the Si inventory from a $MoSi_2$ surface covering the corresponding total area is used for this calculation. The experimental data are superimposed on the theoretical values. The inset enlarges the region for small crystallites with a size <300 nm^2.

projected area for a low- and high-buckled silicene configuration. The lattice constants for two stable buckling configurations from Cahangirov et al.[11] are used to calculate the projected area covered by the lo and high-buckled configuration and determine the corresponding Si-atom densities. Each experimental data point on Figure 5 represents a different crystallite where the total surface area (Rim + SLR) and SLR area were measured. At each total surface area data point a low- and high-buckled silicene area projection was determined as follows.

The number of Si-atoms N_{Si} is calculated for each crystallite size from the total surface area of the crystallite multiplied by the Si-atom density of the h-$MoSi_2$ (0001) plane (eq 1). The Si-atom density projected onto the surface plane is calculated for the low- and high-buckled configurations and yields $D_{Si}(LB)$ = 17.6 atoms/nm^2 and $D_{Si}(HB)$ = 23.6 atoms/nm^2, respectively. N_{Si} is then divided by the Si-atom density of either the low or high-buckled structure resulting in a projected area covered by the SLR $A(LB)$ and $A(HB)$ (eq 2). The surface area covered by the buckled SLR layer is smaller than the crystallite surface area, and the reduction in covered surface area can be related to the buckling. Therefore, each experimental SLR area data point has two comparison data points, one for each buckling configuration.

$$(\text{Total area of Crystallite}) \times (N_{Si} \text{ on h} - MoSi_2(0001)) = N_{Si} \quad (1)$$

$$\frac{N_{Si}}{D_{Si}(LB)} = A(LB) \quad \text{and} \quad \frac{N_{Si}}{D_{Si}(HB)} = A(HB) \quad (2)$$

The experimental data for the SLR agree very well with the low buckling model for silicene. The SLR for the smallest crystallites is close to a high buckling model, but the differences between low and high buckled geometries are rather small for small crystallites and interpretation of buckling phase transformation as a function of crystallite size remains ambiguous. The geometry deduced from this model strongly indicates a preference for a low buckled configuration in the SLR.

STS was performed to probe the electronic structure of the SLR. Figure 6a displays the STM topography image recorded simultaneously with the STS map displayed in Figure 6b and a selection of spectra, which reflect the LDOS (local density of states) of the SLR, rim, and defects (Figure 6c). The spectrum of the Si(001)-(2 × 1) reconstruction is included for comparison. The spectra are averaged over 20−40 individual spectra, and the surface features (SLR, rim, defect) exhibit unique spectral signatures. All observations could be reproduced in several independent experiments. The STS map is depicted for V_{bias} = 1.8 V to maximize color contrast. The LDOS for Si(001)-(2 × 1) shows in agreement with the literature a surface bandgap of ∼0.9 eV, and E_F is positioned close to the valence band edge because the Si substrate is p-doped.

The spectra of the SLR show a small apparent band gap (E_g) of about 0.3 eV, and a small peak positioned at ∼0.3−0.5 eV in the empty states marked by an arrow. These spectral features are observed on crystallites spanning the size range between 340 to 1250 nm^2. The minimum at 0.7 eV (marked by arrow) was previously assigned to the Dirac energy.[13,36,37] However, this assignment is highly speculative and can only be confirmed by future experiments where silicene is integrated as the channel in a gated transistor geometry.[38] The spectra agree well with those presented by Fleurence et al. for silicene on ZrB_2(0001),[16,39] which supports our interpretation of the SLR as silicene. The spectra of the rim area exhibit a distinctly different shape, a band gap of ∼0.3−0.4 eV exceeding the gap of 0.1 eV reported for bulk $MoSi_2$, and an additional peak at about -0.7 eV in the filled states. The rim is therefore not only structurally but also electronically distinct from the SLR. The defect spectra show a mixture of rim and SLR features, which might be due to tunneling current contributions drawn at the side of the STM tip from the SLR in close vicinity.

The most pressing tasks are now the growth of large surface area silicides to form extended silicene domains and the measurement of electronic structure to asses Dirac-type band

DOI: 10.1021/acs.nanolett.6b04065
Nano Lett. 2017, 17, 299−307

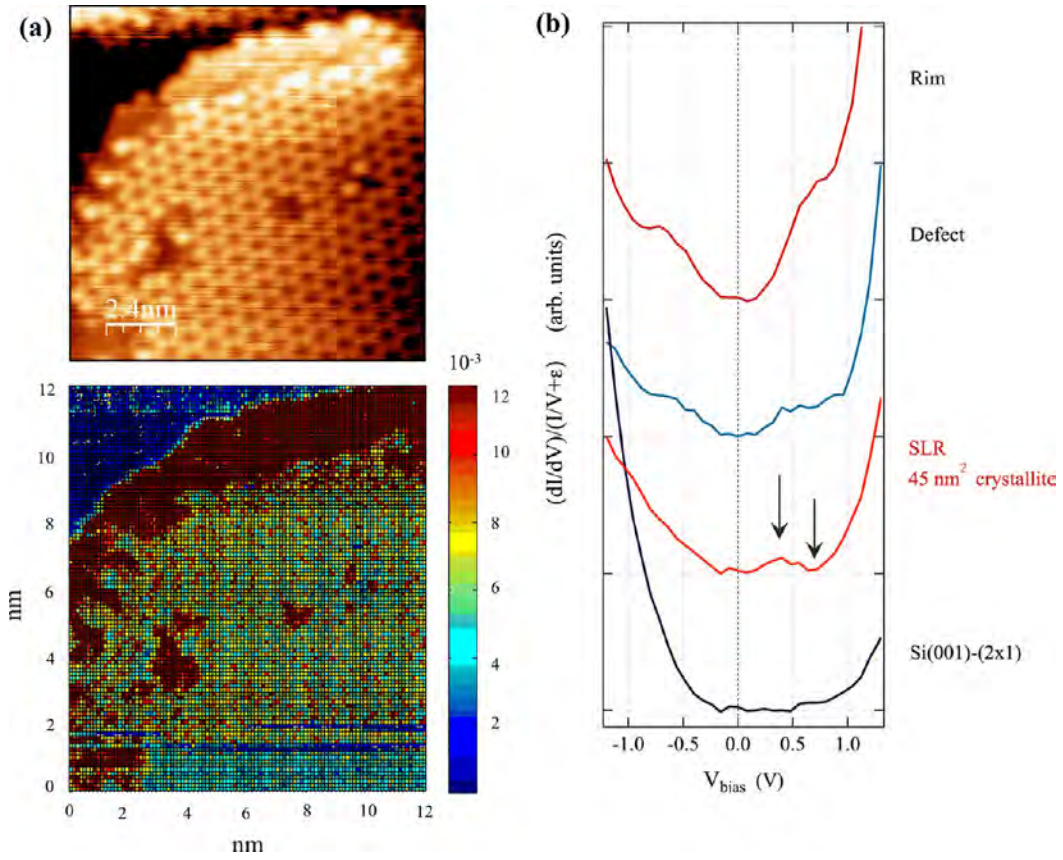

Figure 6. (a) STM image of SLR and corresponding STS map showing the normalized differential conductance at V_{bias} = 1.8 V. (b) Normalized differential conductance spectra $(dI/dV)/(I/V + \varepsilon)$ for Si(001)-(2 × 1), SLR for the crystallite shown in the map, a large defect, and the rim area of the same crystallite. The curves are averaged over 20−40 spectra within the STS map with each spectra being averaged over 100 curves at a single pixel.

structure features. Such data is critical to develop our understanding of silicene−silicide substrate bonding. The latter is the cornerstone for advancing materials development and building a portfolio of suitable substrates. The synthesis of SLR and silicene layers on h-$TMSi_2$(0001) (TM = transition metal) can be subdivided into two tasks: first, the growth of the silicide in a well-defined orientation where the (0001) plane is the terminating surface, and second the formation of silicene layer on this surface. The silicene top layer will therefore have a direct epitaxial relationship to the Si-substrate, which is also seen in the formation of $MoSi_2$ on Si(001). A substantial body of work exists on the epitaxial growth of silicides,[28,40−47] and judicious selection of lattice matched substrates is critical. In addition, use of a semiconducting silicide or at least a silicide like $MoSi_2$ with surface bandgap in [0001][48] is a prerequisite for integration in device structures. However, predictions of a silicene-terminating layers are much more tenuous, and even extensive DFT calculations are still notoriously poor in predicting surface reconstructions for new systems but become very reliable if combined with additional information from experiments.

This study opens the window to a new approach for the synthesis of silicene with a promising path to integration with Si-technology. We have demonstrated that the SLR reconstruction on a hexagonal disilicide (0001) surface is strikingly similar to a low-buckled silicene configuration and provide insight in the electronic structure of the silicene layer. This observation is in contrast to the reconstructions on $ErSi_2$ and $ErSi_{1.7}$, which do not adopt the $(\sqrt{3} \times \sqrt{3})R30°$ surface structure characteristic of a complete silicene layer. The synthesis of the SLR and thus silicene is straightforward and highly reproducible. Improved lattice matching at the h-$MoSi_2$−Si interface through the choice of a different substrate orientation is a promising approach to produce large-area silicene layers. The relaxation of the silicene layer and exposure of the rim area indicates a relatively weak bonding and thus weak electronic coupling between the silicene and silicide. Future experimentation is required to assess the complete electronic structure of the system.

AUTHOR INFORMATION

Corresponding Author

*E-mail: pr6e@virginia.edu.

ORCID

Petra Reinke: 0000-0002-4544-5906

Author Contributions

C.V. and P.R. conceived the experiment, C.V. performed the experiments, and G.R. provided assistance in experiment setup and training. C.V. performed the data analysis, and E.M. assisted in data analysis and guided use of his MATLAB analysis software. C.V. and P.R. led data interpretation and manuscript writing. All authors contributed and agreed on the final manuscript prior to submission.

Notes

The authors declare no competing financial interest.

DOI: 10.1021/acs.nanolett.6b04065
Nano Lett. 2017, 17, 299−307

■ ACKNOWLEDGMENTS

This work is supported by ONR MURI "Understanding Atomic Scale Structure in Four Dimensions to Design and Control Corrosion Resistant Alloys" on Grant N00014-14-1-0675 under the direction of Dr. David Shifler. E.M. acknowledges the support from the National Science Foundation award CHE-1507986 by the Division of Chemistry (Macromolecular, Supramolecular and Nanochemistry).

■ REFERENCES

(1) Miro, P.; Audiffred, M.; Heine, T. An atlas of two-dimensional materials. *Chem. Soc. Rev.* **2014**, *43*, 6537−6554.
(2) Zhu, F.; Chen, W.; Xu, Y.; Gao, C.; Guan, D.; Liu, C.; Qian, D.; Zhang, S.; Lia, J. Epitaxial growth of two-dimensional stanene. *Nat. Mater.* **2015**, *14*, 1020−1025.
(3) Ni, Z.; Liu, Q.; Tang, K.; Zheng, J.; Zhou, J.; Qin, R.; Gao, Z.; Yu, D.; Lu, J. Tunable bandgap in silicene and germanene. *Nano Lett.* **2012**, *12*, 113−8.
(4) Britnell, L.; Gorbachev, R. V.; Jalil, R.; Belle, B. D.; Schedin, F.; Mishchenko, A.; Georgiou, T.; Katsnelson, M. I.; Eaves, L.; Morozov, S.; Perez, N. M. R.; Leist, J.; Geim, A. K.; Novoselov, K. S.; Ponomarenko, L. A. Field-effect tunneling transistor based on vertical graphene heterostructures. *Science* **2012**, *335*, 947−950.
(5) Lembke, D.; Bertolazzi, S.; Kis, A. Single-layer MoS2 electronics. *Acc. Chem. Res.* **2015**, *48*, 100−110.
(6) Lew Yan Voon, L. C.; Zhu, J.; Schwingenschlögl, U. Silicene: Recent theoretical advances. *Appl. Phys. Rev.* **2016**, *3*, 040802.
(7) Mondal, K.; Kamal, C.; Banerjee, A.; Chakrabarti, A.; Ghanty, T. K. Silicene: A Promising Surface to Achieve Morphological Transformation in Gold Clusters. *J. Phys. Chem. C* **2015**, *119*, 3192−3198.
(8) Oughaddou, H.; Enriquez, H.; Tchalala, M. R.; Yildirim, H.; Mayne, A. J.; Bendounan, A.; Dujardin, G.; Ait Ali, M.; Kara, A. Silicene, a promising new 2D material. *Prog. Surf. Sci.* **2015**, *90*, 46−83.
(9) Schwierz, F.; Pezoldt, J.; Granzner, R. Two-dimensional materials and their prospects in transistor electronics. *Nanoscale* **2015**, *7*, 8261−83.
(10) Vogt, P.; De Padova, P.; Quaresima, C.; Avila, J.; Frantzeskakis, E.; Asensio, M. C.; Resta, A.; Ealet, B.; Le Lay, G. Silicene: Compelling Experimental Evidence for Graphenelike Two-Dimensional Silicon. *Phys. Rev. Lett.* **2012**, *108*, 155501.
(11) Cahangirov, S.; Topsakal, M.; Aktürk, E.; Şahin, H.; Ciraci, S. Two- and One-Dimensional Honeycomb Structures of Silicon and Germanium. *Phys. Rev. Lett.* **2009**, *102*, 236804.
(12) Lee, C.-C.; Fleurence, A.; Friedlein, R.; Yamada-Takamura, Y.; Ozaki, T. First-principles study on competing phases of silicene: Effect of substrate and strain. *Phys. Rev. B: Condens. Matter Mater. Phys.* **2013**, *88*, 165404.
(13) Feng, B.; Ding, Z.; Meng, S.; Yao, Y.; He, X.; Cheng, P.; Chen, L.; Wu, K. Evidence of silicene in honeycomb structures of silicon on Ag(111). *Nano Lett.* **2012**, *12*, 3507−11.
(14) Prévot, G.; Bernard, R.; Cruguel, H.; Curcella, A.; Lazzeri, M.; Leoni, T.; Masson, L.; Ranguis, A.; Borensztein, Y. Formation of silicene on silver: Strong interaction between Ag and Si. *Phys. Status Solidi B* **2016**, *253*, 206−217.
(15) Švec, M.; Hapala, P.; Ondráček, M.; Merino, P.; Blanco-Rey, M.; Mutombo, P.; Vondráček, M.; Polyak, Y.; Cháb, V.; Martín Gago, J. A.; Jelínek, P. Silicene versus two-dimensional ordered silicide: Atomic and electronic structure of Si-(19 × 19)R23.4°/Pt(111). *Phys. Rev. B: Condens. Matter Mater. Phys.* **2014**, *89*, 201412.
(16) Fleurence, A.; Friedlein, R.; Ozaki, T.; Kawai, H.; Wang, Y.; Yamada-Takamura, Y. Experimental Evidence for Epitaxial Silicene on Diboride Thin Films. *Phys. Rev. Lett.* **2012**, *108*, 245501.
(17) Chiappe, D.; Scalise, E.; Cinquanta, E.; Grazianetti, C.; van den Broek, B.; Fanciulli, M.; Houssa, M.; Molle, A. Two-dimensional Si nanosheets with local hexagonal structure on a MoS(2) surface. *Adv. Mater.* **2014**, *26*, 2096−101.
(18) Meng, L.; Wang, Y.; Zhang, L.; Du, S.; Wu, R.; Li, L.; Zhang, Y.; Li, G.; Zhou, H.; Hofer, W. A.; Gao, H. J. Buckled silicene formation on Ir(111). *Nano Lett.* **2013**, *13*, 685−90.
(19) Zoethout, E.; Louis, E.; Bijkerk, F. Real-space insight in the nanometer scale roughness development during growth and ion beam polishing of molybdenum silicon multilayer films. *Appl. Surf. Sci.* **2013**, *285*, 293−299.
(20) Feenstra, R. M. A prospective: Quantitative scanning tunneling spectroscopy of semiconductor surfaces. *Surf. Sci.* **2009**, *603*, 2841−2844.
(21) Nečas, D.; Klapetek, P. *Open Physics* **2012**, *10*, 181.
(22) Horcas, I.; Fernandez, R.; Gomez-Rodriguez, J. M.; Colchero, J.; Gomez-Herrero, J.; Baro, A. M. WSxM. *Rev. Sci. Instrum.* **2007**, *78*, 013705.
(23) Bedrossian, P. J. Nucleation and ordering of $MoSi_2$ on Si(100). *Surf. Sci.* **1995**, *322*, 73−82.
(24) Perio, A.; Torres, J.; Bomchil, G.; Arnaud d'Avitaya, F.; Pantel, R. Growth of MoSi2 with preferential orientation on (100) silicon. *Appl. Phys. Lett.* **1984**, *45*, 857.
(25) Perio, A.; Torres, J. Thermal evolution of molybdenum disilicide grown on (100) silicon under ultrahigh vacuum conditions. *J. Appl. Phys.* **1986**, *59*, 2760.
(26) Lin, W. T.; Chen, L. J. Localized epitaxial growth of MoSi2 on silicon. *J. Appl. Phys.* **1986**, *59*, 1518.
(27) Nolph, C. A.; Simov, K. R.; Liu, H.; Reinke, P. Manganese nanostructures on Si(100)-(2 × 1) surfaces: temperature-driven transition from wires to silicides. *J. Phys. Chem. C* **2010**, *114*, 19727−19733.
(28) Lin, W. T.; Chen, L. J. Localized epitaxial growth of hexagonal and tetragonal MoSi2 on (111) Si. *Appl. Phys. Lett.* **1985**, *46*, 1061.
(29) Rogero, C.; Koitzsch, C.; González, M. E.; Aebi, P.; Cerdá, J.; Martín-Gago, J. A. Electronic structure and Fermi surface of two-dimensional rare-earth silicides epitaxially grown on Si(111). *Phys. Rev. B: Condens. Matter Mater. Phys.* **2004**, *69*, 045312.
(30) Sanna, S.; Dues, C.; Schmidt, W. G.; Timmer, F.; Wollschläger, J.; Franz, M.; Appelfeller, S.; Dähne, M. Rare-earth silicide thin films on the Si(111) surface. *Phys. Rev. B: Condens. Matter Mater. Phys.* **2016**, *93*, 195407.
(31) Wetzel, P.; Saintenoy, S.; Pirri, C.; Bolmont, D.; Gewinner, G. Surface states and reconstruction of epitaxial $\sqrt{3} \times \sqrt{3}$ R30° Er silicide on Si(111). *Phys. Rev. B: Condens. Matter Mater. Phys.* **1994**, *50*, 10886−10892.
(32) Wetzel, P.; Saintenoy, S.; Pirri, C.; Bolmont, D.; Gewinner, G.; Roge, T. P.; Palmino, F.; Savall, C.; Labrune, J. C. STM investigation of 2- and 3-dimensional Er disilicide grown epitaxially on Si(111). *Surf. Sci.* **1996**, *355*, 13−20.
(33) Baptist, R.; Ferrer, S.; Grenet, G.; Poon, H. C. Surface crystallography ofYSi2−xfilms epitaxially grown on Si(111): An x-ray photoelectron diffraction study. *Phys. Rev. Lett.* **1990**, *64*, 311−314.
(34) Iancu, V.; Kent, P. R.; Hus, S.; Hu, H.; Zeng, C. G.; Weitering, H. H. Structure and growth of quasi-one-dimensional YSi2 nanophases on Si(100). *J. Phys.: Condens. Matter* **2013**, *25*, 014011.
(35) Roge, T. P.; Palmino, F.; Savall, C.; Labrune, J. C.; Wetzel, P.; Pirri, C.; Gewinner, G. Surface reconstruction ofErSi1.7(0001) investigated by scanning tunneling microscopy. *Phys. Rev. B: Condens. Matter Mater. Phys.* **1995**, *51*, 10998−11001.
(36) Fleurence, A.; Yoshida, Y.; Lee, C. C.; Ozaki, T.; Yamada-Takamura, Y.; Hasegawa, Y. Microscopic origin of the π states in epitaxial silicene. *Appl. Phys. Lett.* **2014**, *104*, 021605.
(37) Chen, L.; Liu, C. C.; Feng, B.; He, X.; Cheng, P.; Ding, Z.; Meng, S.; Yao, Y.; Wu, K. Evidence for Dirac fermions in a honeycomb lattice based on silicon. *Phys. Rev. Lett.* **2012**, *109*, 056804.
(38) Zhang, Y.; Brar, V. W.; Wang, F.; Girit, C.; Yayon, Y.; Panlasigui, M.; Zettl, A.; Crommie, M. F. Giant phonon-induced conductance in scanning tunneling spectroscopy of grate-tunable graphene. *Nat. Phys.* **2008**, *4*, 627−630.
(39) Fleurence, A.; Gill, T. G.; Friedlein, R.; Sadowski, J. T.; Aoyagi, K.; Copel, M.; Tromp, R. M.; Hirjibehedin, C. F.; Yamada-Takamura,

DOI: 10.1021/acs.nanolett.6b04065
Nano Lett. 2017, 17, 299−307

Y. Single-domain epitaxial silicene on diboride thin films. *Appl. Phys. Lett.* **2016**, *108*, 151902.
(40) Schlesinger, M. E. Thermodynamics of solid transition-metal silicides. *Chem. Rev.* **1990**, *90*, 607−628.
(41) Johnson, C. D.; Anderson, K.; Gromko, A. D.; Johnson, D. C. Variation of nucleation energy of molybdenum silicides as a function of the composition of an amorphous precursor. *J. Am. Chem. Soc.* **1998**, *120*, 5226−5232.
(42) Borisenko, V. E. *Semiconducting Silicides - Springer series in materials science*; Springer: Berlin, 2000; Vol. *39*.
(43) Chen, L. J.; Tu, K. N. Epitaxial growth of transition-metal silicides on silicon. *Mater. Sci. Rep.* **1991**, *6*, 53−140.
(44) Cheng, J. Y.; Cheng, H. C.; Chen, L. J. Cross-sectional transmission electron microscope study of the growth kinetics of hexagonal MoSi2 on (001)Si. *J. Appl. Phys.* **1987**, *61*, 2218.
(45) Guivarc'h, A.; Auvray, P.; Berthou, L.; Le Cun, M.; Boulet, J. P.; Henoc, P.; Pelous, G.; Martinez, A. Reaction kinetics of molybdenum thin films on silicon (111) surface. *J. Appl. Phys.* **1978**, *49*, 233−237.
(46) Perio, A.; Torres, J. Thermal evolution of molybdenum disilicide grown on (100) silicon under ultrahigh vacuum conditions. *J. Appl. Phys.* **1986**, *59*, 2760−2764.
(47) Perio, A.; Torres, J.; Bomchil, G.; Arnaud d'Avitaya, F.; Pantel, R. Growth of MoSi2 with preferential orientation on (100) silicon. *Appl. Phys. Lett.* **1984**, *45*, 857−859.
(48) Filonov, A. B.; Tralle, I. E.; Dorozhkin, N. N.; Migas, D. B.; Shaposhnikov, V. L.; Petrov, G. V.; Anishichik, V. M.; Borisenko, V. E. Semiconducting properties of hexagonal Chromium, Molybdenum and Tungsten Disilicides. *Phys. Status Solidi B* **1994**, *186*, 209−215.

DOI: 10.1021/acs.nanolett.6b04065
Nano Lett. 2017, 17, 299−307